J. of Supercritical Fluids 110 (2016) 47–55

Contents lists available at ScienceDirect

The Journal of Supercritical Fluids

journal homepage: www.elsevier.com/locate/supflu

Optimization and modelling of the supercritical CO_2 deposition of Co_xO_y nanoparticles in MCM41

S. Aspromonte [a], A. Sastre [b], A. Boix [a], M.J. Cocero [b], E. Alonso [b,*]

[a] Instituto de Investigaciones en Catálisis y Petroquímica – INCAPE (FIQ, UNL-CONICET), Santiago del Estero 2829, 3000 Santa Fe, Argentina
[b] High Pressure Processes Group – Chemical Engineering and Environmental Technology Department, University of Valladolid, C/ Dr. Mergelina s/n, 47011 Valladolid, Spain

ARTICLE INFO

Article history:
Received 4 October 2015
Received in revised form
23 November 2015
Accepted 23 November 2015
Available online 25 December 2015

Keywords:
Supercritical deposition
Cobalt oxide
Mesoporous silica
Cobaltocene
MCM41

ABSTRACT

Nanocomposites of cobalt oxide on mesoporous silica support (Co/MCM41) have been synthesized by supercritical fluid reactive deposition (SCFRD) using cobaltocene ($CoCp_2$) as precursor. The study of adsorption isotherm for $CoCp_2$ on MCM41 at 70 °C and 11 MPa has revealed an unfavourable adsorbate–adsorbent system with a maximum load of 43 mgCo/gMCM41. Thus, an in situ thermal decomposition of precursor is necessary to obtain higher loadings of active phase. The modelling of the SCFRD process reveals that dissolution is very fast compared to the adsorption of cobaltocene on MCM41, and that Co content is maximum after 1 h of decomposition at 200 °C and 14 MPa. The composite material with 4.3 wt.% Co has a BET surface area of 1034 $m^2\,g^{-1}$, a pore size of 3.9 nm and metal nanoparticles of 20–30 nm. This load can be increased by successive batches of 1 h.

1. Introduction

Mesoporous materials, with uniform and tailorable pore dimensions and high specific surface, are currently employed in a number of applications that include catalysis [1,2] and their use as templates for controlling the aspect ratio of quantum-confined nanoparticles and nanowires [3] among others. For many of these applications, it is important that the nanoparticles should be small in size and well-dispersed on a robust support of high surface area. MCM41 is one of the most extensively studied meso-structure materials, since it was first synthesized by Mobil Corporation in 1992 [4]. MCM41 is a mesoporous-silica material that contains unidirectional channels arranged in a regular hexagonal pattern in the range of 20–100 Å. In the recent literature, it can be found attempts to insert metals, such as, Cu, Ca, Mg, Ti, Cr, Mn or Fe into the MCM41 framework, and this incorporation has been generally performed by wet impregnation or co-precipitation [5–10].

Supercritical fluids (SCFs) have been used to incorporate metallic oxide particles and films into a wide variety of supports [11–15]. In the supercritical fluid deposition (SCFD) process, an organometallic precursor is dissolved in supercritical carbon dioxide ($scCO_2$), and after impregnation of the support, precursor is thermally decomposed or chemically reduced, and deposition of metal or metal oxide particles takes place on the mesoporous support. This technique was developed by Watkins and McCarthy [16] and it took advantage of the excellent physical properties of $scCO_2$, which are easily adjustable with small variations of pressure and/or temperature. The low viscosity, high diffusivity and zero surface tension of $scCO_2$ achieve better penetrating and wetting of pores than conventional liquid solvents. Furthermore, simple removal from the substrate by depressurization avoids problems of solvent residues or pore collapse, and it can be performed in a one-pot process, reducing operation times [17,18]. The technique can be examined under three main categories: (i) the dissolution of the metallic precursor in the SCF, (ii) the adsorption or sorption of the metallic precursor on the substrate, and (iii) decomposition of the precursor [11,19,20]. According to a recent work [21] that summarizes many methods of insertion of different active phase nanoparticles in mesoporous silica materials, the supercritical fluid reactive deposition (SCFRD) process seems to lead the most homogeneous materials with nanoparticles well-dispersed on the support.

Cobalt is one of the most deeply investigated transition metals for heterogeneous catalytic applications. In the form of supported single element or alloys, cobalt is an interesting active metal for the catalysis of several reactions ranging from catalytic combustion [22,23], steam reforming [24,25], ammonia synthesis [26], Fischer–Tropsch (FT) synthesis [27–30], and abatement of NOx

* Corresponding author.
E-mail address: ealonso@iq.uva.es (E. Alonso).

http://dx.doi.org/10.1016/j.supflu.2015.11.026
0896-8446/

[31–33] and CO [34]. Narrowly, (n,m)-distributed single-walled carbon nanotubes (SWNTs) have been obtained with cobalt-incorporated MCM41 (Co/MCM41) catalysts [35,36]. Up to our knowledge, there are few works about the SCFD of cobalt. In this sense, Hunde and Watkins [37] reported the deposition of Co and Ni films directly onto a native oxide of Si wafers and onto TaN and TiN films supported on Si wafers, without the need of a catalytic layer, by H_2 reduction of cobaltocene ($CoCp_2$). In this work, dissolution of $CoCp_2$ in the CO_2 was performed at 70 °C and 11.0 MPa for 1 h and deposition time was 30 min in all cases. Reduction temperature of cobaltocene was varied in the range 285–320 °C and the pressure was modified between 22.0 and 26.0 MPa. No significant deposition was observed below 280 °C and the operational times of the two steps were not varied. Up to now, only a few organometallic compounds on porous support have been studied in $scCO_2$. The adsorption equilibrium of [$Pd(hfac)_2$] on silica SBA-15 and the influence of the temperature, pressure and density in the process has been examined [38]. The adsorption isotherms of [$Pt(CODMe_2)$] on different supports, such as carbon aerogels, silica gel tablets or monolithic silica have been reported [39,40].

Our research group has shown the deposition of 1 and 5 wt.% Co on mesoporous MCM41 and AlMCM41 substrates with supercritical CO_2 at 200 °C and 11 MPa [41]. Due to the promising results obtained, the present work goes deep to the synthesis in order to understand the process and to optimize the operational conditions and model the reactive deposition process with $scCO_2$.

Hence, the aim of the present work is to optimize the deposition of cobalt oxide on the MCM41 mesoporous substrate using cobaltocene ($CoCp_2$) as precursor and CO_2 as supercritical fluid. For this purpose, three consecutive stages are examined: (i) determination of adsorption isotherms of $CoCp_2$ on MCM41 support, (ii) study of operational variables: time, pressure and temperature in the SCFRD method of synthesis during adsorption and precursor decomposition stages and (iii) physicochemical characterization of the solids by different techniques such as FTIR spectroscopy, X-ray diffraction (XRD) and inductively coupled plasma (ICP-OES).

2. Materials and methods

2.1. Organometallic precursor: cobaltocene

Cobalt(II)bis-(η^5ciclopentadienil), also known as cobaltocene ($CoCp_2$) has been used as cobalt precursor in the present work because it is known to be highly soluble in $scCO_2$ [40] and it has been used in the cobalt deposition of high purity thin films directly on silicon oxide [37]. $CoCp_2$ was provided by Sigma–Aldrich and used as received.

2.2. Synthesis of MCM41 support

MCM41 support was synthesized following the method of Szegedi et al. [42]. A solution of surfactant (C_{16}TMABr) was prepared by continuous mixing with de-ionized water and absolute ethanol at room temperature. The pH of the solution was adjusted by adding an aqueous ammonia solution (29 wt.%). Then, tetraethylorthosilicate (TEOS) was added dropwise in a couple of minutes. The molar composition of the resulting gel mixture was $TEOS{:}0.3C_{16}TMABr{:}11NH_3{:}144H_2O{:}58EtOH$.

The obtained support was filtered, thoroughly washed with de-ionized water and dried for 12 h at 60 °C. The template was removed by calcination in flow of air at 550 °C during 6 h.

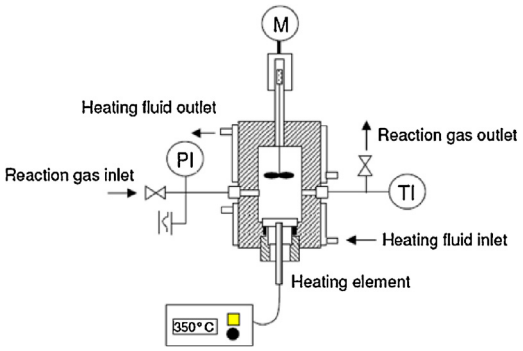

Fig. 1. Flow sheet of the experimental device for adsorption isotherms determination.

2.3. Experimental set-up for determination of adsorption isotherms

The determination of adsorption isotherms was carried out in a high pressure reaction chamber. A scheme of the experimental set-up is reported in Fig. 1. The chamber, HP HD300 from Eurotechnica GmbH, is built on SS316-Ti and it has an internal volume of 25 ml, supporting 30 MPa and 150 °C as maximum operating conditions. A magnetic driven agitator (12 VDC with transformer 230 VAC) is installed at the top of the reaction chamber in order to ensure a homogeneous medium. The temperature of the vessel was controlled by means of an electrical jacket (230 VAC; 50/60 Hz) connected to a digital display and NiCr—Ni thermocouple with a ±0.1 °C accuracy, while the pressure inside the chamber is measured by a pressure gauge between 0.1 and 40 MPa.

At the beginning, a known amount of support and precursor are introduced at the bottom of the chamber in two separate perforated containers. The CO_2 is pumped with a dosing pump Milton Roy Dosapro, MILROYAL D (up to 0.6 L/h and 24 MPa) and heated up to operational conditions. Experiments were carried out at constant temperature (70 °C) for 24 h, carrying the amount of precursor at different CO_2 pressures [39,40]. After that, the fluid is slowly depressurized in order to prevent the sweeping along particles and recover the products for further analysis.

2.4. SCFRD of $CoCp_2$ on MCM41

The deposition experiments were carried out in batch process in a home-made high pressure vessel made up of stainless steel with an internal volume of 100 ml. The experimental set-up, given in Fig. 2, operates up to 30 MPa and 400 °C as maximum allowable working conditions. A dosing pump Milton Roy Dosapro (flow rate up to 6.2 L/h and 33 MPa maximum pressures) was used to feed the CO_2 into the reactor.

At the beginning of each experiment, 150 mg of support and 100 mg of organometallic precursor were placed into the vessel, separated by wire mesh to allow the circulation of $scCO_2$ and avoid their direct contact (Fig. 3). The reactor is equipped with two walls electrical resistances (250 W) placed at the bottom to promote the convective flow of $scCO_2$. The process temperature is controlled by a K-type thermocouple located inside the reactor and connected to a PID controller (Desin Instruments 2100 BS) acting on this electrical resistances. A pressure transmitter (ATSA TPR-14/STD) located at the top of the reactor is used for the continuous registration of pressure. Wall temperature is also measured (Fig. 2).

Deposition experiments were carried out in batch operation divided in two consecutive stages. During the first step, precursor is dissolved by $scCO_2$ and adsorbed onto the support from the fluid medium. Experiments were conducted at 70 °C and 11 MPa in this first stage, and time was varied between 1 and 3 h, in order to study

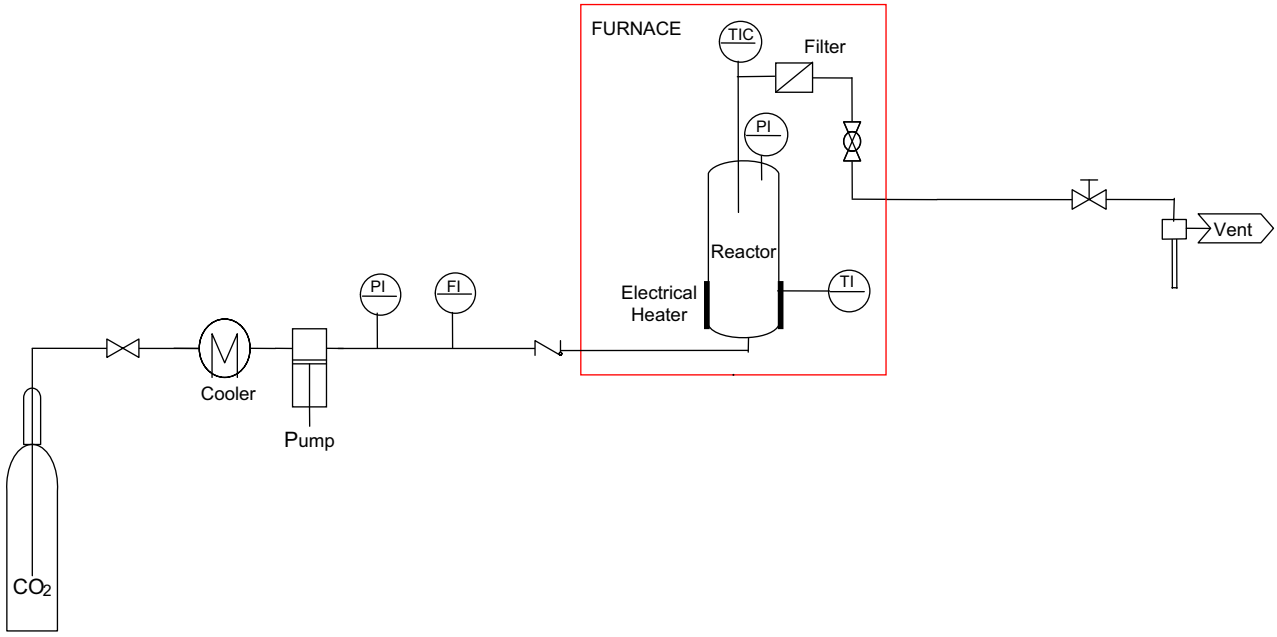

Fig. 2. Experimental device for the synthesis by SCFRD (batch process).

the influence of time in this first stage of the deposition method. After this dissolution–adsorption step, temperature is increased up to 200 °C to break down the organometallic compound, with the subsequent precipitation of the metallic nanoparticles during the desired decomposition time. Afterwards, the system is isochorically cooled down to subcritical conditions, and CO_2 is slowly released from the reactor over a period of 30 min, which implies a slowly depressurization to atmospheric pressure to avoid drag metallic nanoparticles which are adsorbed over the support surface. Pressures between 9 and 30 MPa and time in the range 1–3 h were varied in this second stage for their study.

2.5. Physicochemical characterization techniques

X-ray diffractograms were recorded by Philips PW 1710, applying monochromatized Cu Kα radiation (40 kV, 35 mA). The mean crystallite size of the cobalt oxide nanoparticles was estimated by the Debye–Scherrer equation [39].

Nitrogen physisorption measurements were carried out at −196 °C using a Micromeritics Accusorb 2100E instrument. The samples were previously degassed at 320 °C under medium vacuum atmosphere for 8 h. There are many methodologies based on the Kelvin equation, which describes the capillary condensation produces in the mesopores. Among them, the method described by Barker, Joiyner and Halenda (BJH method) is commonly used to determine the volume and size distribution of mesopores [40].

FTIR experiments were performed with Bruker Tensor 27 spectrometer with an ATR "Golden Gate" over 4000–400 cm^{-1} range at the resolution of 4 cm^{-1} and 64 scans. The MCM41 support and Co/MCM41 samples were diluted in KBr (1/200) and self-supported wafer, which was introduced into the sample holder of the FTIR equipment. Thermogravimetric analyzes (TGA) were used to determine the decomposition temperature of the cobalt precursor and the residual deposits remaining. For this purpose, a Mettler Toledo thermobalance SAE, model TGA/SDTA 851e, which was equipped with a horizontal furnace with a maximum temperature of 1100 °C in air flow was used.

The chemical composition of the metallic species in the synthesized materials was determined by ICP-OES with Perkin Elmer Optima 2100DV equipment. Acid digestion of the solid samples was used.

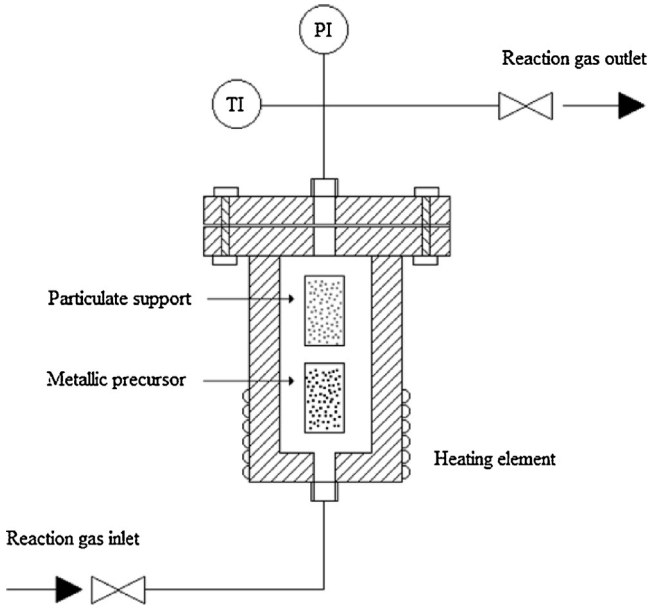

Fig. 3. Detail of the distribution of raw materials (support and precursor) within deposition chamber.

3. Results and discussion

3.1. Adsorption isotherms of $CoCp_2$ on MCM41

To achieve a good understanding of nanoparticles deposition process by using supercritical fluids is fundamental the comprehension of the adsorption process at supercritical conditions. In our case, the adsorption of a cobalt organometallic precursor of the family of the metallocenes ($CoCp_2$) on the mesoporous MCM41 support in supercritical CO_2 was studied.

Fig. 4 shows the adsorption isotherm for $CoCp_2$ on MCM41 at 70 °C and 11 MPa. Under these conditions the estimated solubility of cobaltocene in $scCO_2$ is around 350 mg L^{-1}, according to the literature data [43].

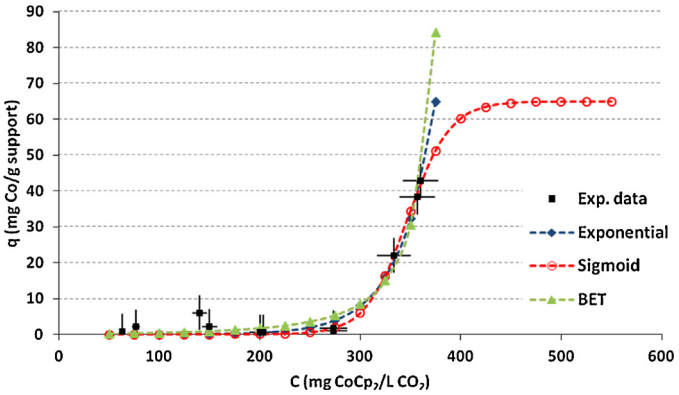

Fig. 4. Experimental data (■) and fit by exponential (♦), sigmoid (○) and BET (▲) correlations for adsorption isotherms of $CoCp_2$ on MCM41 at 70 °C and 11 MPa.

Table 1
Fitted model parameters and average deviation for the adsorption equilibrium of $CoCp_2$ on MCM41 in $scCO_2$.

Model	Isotherm/70 °C, 11 MPa
Exponential	
A	0.0017
B	1.028
MSE	1.68
Sigmoid	
q_s (mg g^{-1})	64.89
a (L mg^{-1})	0.048
b	−16.786
MSE	1.41
BET	
K_{bet} (L mg^{-1})	0.0083
Q_m (mg g^{-1})	109.93
C_m (mg L^{-1})	414.60
MSE	2.08

As it is shown in Fig. 4, the metallic loading in the solid (q) is practically non-existent for a wide range of concentrations up to 250 mg L^{-1}. Above this value, the adsorption capacity increases exponentially. The shape of the isotherm is concave upward and presents a vertical asymptote corresponding to the vapor pressure of the adsorbate (i.e. condensation) [44]. This means that the second layer is more strongly adsorbed than the first one, an effect related to the existence of attractive interactions between the adsorbed molecules. In these cases, however, the adsorbent still has finite saturation capacity and the isotherm could have an horizontal asymptote [45]. This behaviour is characteristic when the adsorbate–adsorbent interaction is low or conversely, there is a greater affinity for the fluid medium (type III), at least in the entire concentrations range investigated, from 0 to close to the saturation of fluid phase. Although this type of isotherm is unusual, it can be found several examples in the literature, such as bromine or iodine on silica gel, or water over some hydrophobic rubbers, plastics, synthetic fibres or graphitized carbon [46].

On the other hand, competition between the solvent and the solute for the support sites may also be possible, especially for systems involving low solubility or weak adsorbing solute species [47]. However, this phenomenon may be diminished at supercritical conditions, since the transport coefficients are enhanced [48]. Besides, MCM41 surface does not interact very strongly with CO_2 according to others authors [49,50].

3.2. Adsorption isotherms modelling

Several authors have been tried to predict isotherms of type III with anti-Langmuir models [45,51]. This means that it could be modelled by using a Langmuir model with negative association equilibrium constant [45], but although this modification provides good fits, its parameters lack physical sense.

Another option is the use of an exponential equation as the following expression:

$$q = A \cdot B^{C} \tag{1}$$

where A and B are constants, while C is the concentration of the organometallic precursor in the fluid phase (mg L^{-1}). Worth mentioning that this model is only recommendable for low concentrations, since at very high initial concentrations, it predicts depositions that tend to infinity.

To solve these drawbacks, the isotherms describing best this type of behaviour are generally referred to an S-shape isotherm and they are often best modelled using the quadratic isotherm model, where the initial curvature is negative. The simplest equation of this kind of models is known as sigmoid function as follow:

$$q = \frac{q_S}{1 + \exp(-a \cdot C - b)} \tag{2}$$

where q_s is the adsorptive capacity, a is related to the saturation concentration, and b depends on the minimum concentration which must be overcome to start adsorption.

On the other hand, among all these options, BET adsorption isotherm model [52] is the most used alternative to study this kind of systems: whose equation is able to reproduce any singularity in adsorption process, even different kinds of isotherms as a function of the relationship between its parameters. Thus, the equation is expressed as follows:

$$q = \frac{Q_m \cdot C_e}{(C_m - C_e) \cdot [1 + (K_{bet} - 1) \cdot (C_e/C_m)]} \tag{3}$$

where q is the equilibrium adsorption capacity (mg g^{-1}), Q_m is the theoretical isotherm monolayer capacity (mg g^{-1}), K_{bet} is the BET adsorption isotherm constant (L mg^{-1}) and C_m is the adsorbate monolayer concentration (mg L^{-1}).

To adjust the isotherm parameters and conclude which is the best model for describing the equilibrium, it is necessary to calculate the mean squared error, defined in Eq. (4):

$$\text{MSE} = \frac{1}{n}\sum_{i=1}^{n} \left| q_i^{exp} - q_i^{calc} \right|^2 \tag{4}$$

Fig. 4 shows the adjustment provided by the models described afore mentioned and Table 1 summarizes the characteristic parameters and mean squared error of each of them.

All the models fit nearly within the range of studied concentration, with a MSE ≤ 2; however, predictions about the progression of the adsorption process vary significantly from each other. The exponential equation works nicely as empirical model with only two constants, quickly and easily; nevertheless, no valid information is achieved from the analysis of its parameters.

On the other hand, BET isotherm provides similarly to the exponential curve, that is a multilayer adsorption, but in this case, attending to its characteristic parameters, it is possible to note several important aspects. BET adsorption isotherm constant (K_{bet}) is slightly larger than the pre-exponential factor in the previous model, which results in superior metallic loadings as it can be observed at high concentration in Fig. 4. This means that the affinity of the metallocene by itself and the crystal growth rate predicted by this model are higher.

Also, according to the results shown in Table 1, it is possible to obtain homogeneous monolayer depositions with loadings around 110 mg g^{-1} (theoretical monolayer capacity); and that to achieve

this goal, an initial precursor concentration higher than 415 mg g^{-1} is needed.

Conversely, sigmoid function predicts a completely different behaviour. In the first place, this model assumes that there exists a maximum concentration at which the substrate is saturated, and therefore it cannot be obtained depositions higher than 65 mg g^{-1}, well below even the prognosticated monolayer deposition by BET model. Nonetheless, the adsorbate saturation concentration C_s, at which this loading is achieved, is very close to that estimated by BET isotherm, around 420 mg g^{-1}.

All in all, we are dealing with an adsorbate–adsorbent system which is not favourable under current conditions for supercritical fluid deposition process (SCFD). For this reason, it is necessary including a reaction step (SCFRD) in order to promote the precipitation of metallic nanoparticles over the support surface after the rupture of the precursor in the fluid phase. This rupture can be promoted by a reducing agent or by thermal decomposition. In this work, an increase of the temperature above the decomposition temperature of the precursor was chosen. While precipitation, the organic portion remains dissolved in the supercritical phase. The whole process optimization is developed in the next section.

3.3. Operational conditions of SCFRD process

In the previous section, it has been concluded that for the deposition of cobalt from $CoCp_2$ on MCM41 is not enough a simple exposure of a solution of the precursor over the support, since the adsorption is not favourable. For this reason, the supercritical fluid reactive deposition (SCFRD) has been performed. Different tests were performed in order to optimize the process, analyzing its operational variables and their consequential effects, such as pressure, temperature and time.

3.3.1. Selection of decomposition temperature

The decomposition temperature of the cobaltocene was determined by thermogravimetric analysis (TGA) under N_2 flow at atmospheric pressure. In this way, the optimal temperature range for the deposition of nanoparticles from $CoCp_2$ on the support was identified. The thermogram obtained for the pure cobaltocene (not shown), exhibits a total mass loss of 90%, starting at about 110 °C and finishing at 215 °C, with a maximum at 192 °C. On this basis, the operating temperature for the decomposition step of the SCFRD process was set to 200 °C. Furthermore, FTIR technique was used in order to verify the molecular structure of pure precursor and, after its decomposition in $scCO_2$ at 200 °C and 11.0 MPa for 3 h (Fig. 5). The vibrational spectra of bis(η^5-cyclopentadienyl) metal complex (Cp_2M) have been studied in detail and reported in the literature [53]. Several signals assigned to different vibrational modes of the $CoCp_2$ molecule are observed in Fig. 5. The bands at 861 and 774 cm^{-1} are attributed to the different vibrational modes of stretching of C—H bond of cyclopentadiene. These bands are reported for the $CoCp_2$ precursor in its basal state (spectrum a). Moreover, at low wavenumber regions, a peak appears at 664 cm^{-1}, which is related to the vibrational deformations caused by the bond Cp—Co—Cp between the cobalt and the ligand [54,55]. However, significant differences were observed after the exposition of the cobaltocene to $scCO_2$ at 200 °C and 11.0 MPa. The spectrum of the $CoCp_2$ treated under these conditions (Fig. 5, spectrum b), showed a shift of the signals at 774 and 664 cm^{-1} towards lower wavenumbers after the contact of metal precursor with $scCO_2$, which could be due to the rupture of the Cp—Co—Cp bonds. According to these evidences, it was demonstrated that at 11.0 MPa and 200 °C, the decomposition of cobaltocene in $scCO_2$ is reached. Therefore, a temperature of 200 °C for the decomposition and deposition of nanoparticles on the MCM41 support was selected.

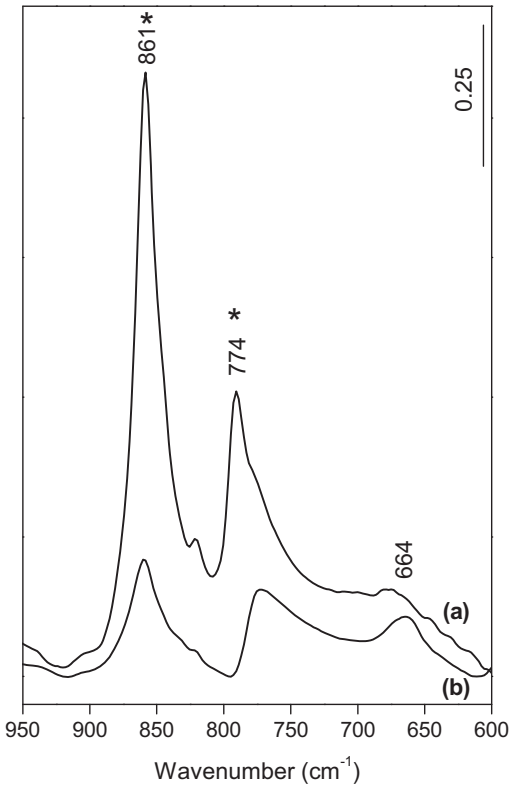

Fig. 5. FTIR spectra of $CoCp_2$ (a) pure and (b) after exposure to $scCO_2$ at 200 °C and 11.0 MPa. *Main signals of $CoCp_2$ in its basal state.

3.3.2. Effect of pressure on the decomposition and deposition stage

In order to select the suitable pressure for the decomposition stage, a series of experiments were performed by changing this variable between 9 and 20 MPa. For these set of experiments, time was maintained in 3 h. Table 2 summarizes these results, where it can be observed that this process presents a maximum of cobalt loading for a pressure of 14.0 MPa, hence this value has been chosen as pressure for the second stage. According to these preliminary results, the conditions for the first step have been fixed at 70 °C and 11 MPa, while for the thermal degradation of the precursor, the temperature was fixed at 200 °C and the pressure at 14 MPa. Probably, under these conditions there is a competition among precursor solubilization, decomposition kinetics, and adsorption of precursor and/or intermediates. The dissolution is favoured by pressure, whereas thermal decomposition is a reaction that implies an increase in the number of molecules in gas phase and therefore, it is favoured by low pressures. From these results, the maximum loading of cobalt takes place at a pressure of 14 MPa, what means that below this value, dissolution is controlling the step, whereas above this value is the decomposition reaction the controlling mechanism.

Table 2
Metallic loading deposited by SCFRD. Conditions: 3 h (70 °C, 11 MPa) + 3 h (200 °C, different pressures).

Pressure (MPa)	wt.% Co[a]
9	2.61
11	2.52
14	2.90
17	2.55
20	2.08

[a] Content of cobalt determined by ICP-OES.

Table 3
Effect of time in the amount of cobalt deposited during the first and second stage of SCFD on Co/MCM41 material.

	Time (h)	wt.% Co[a]
Stage 1 (70 °C, 11.0 MPa)	1	0.05
	2	0.07
	3	0.08
Stage 2 (200 °C, 14.0 MPa)	1	2.90
	2	3.30
	3	3.20
Stage 1 + Stage 2 (70 °C, 11.0 MPa) + (200 °C, 14.0 MPa)	3 + 1	4.30

[a] The Co content was determined by ICP-OES (wt.%).

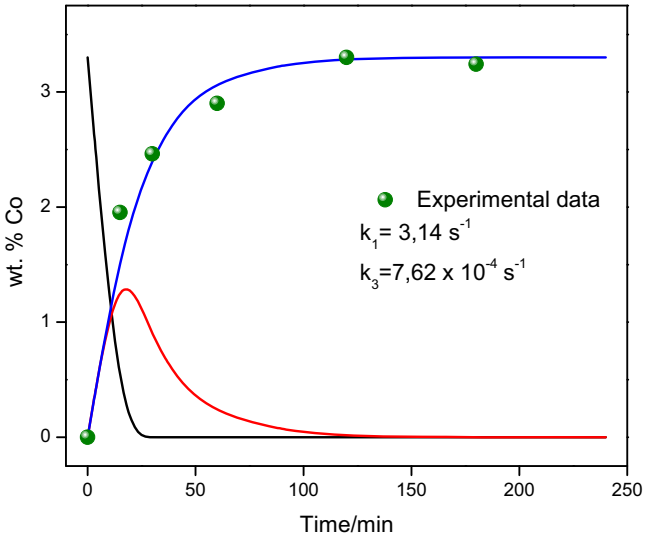

Fig. 6. Simulation curves for SCFRD as serial reaction kinetics: (●) experimental values; (a) evolution of precursor in solid state; (b) precursor dissolved in sc-CO_2; and (—) metallic nanoparticles adsorbed on the support.

3.3.3. Kinetics of the process: effect of time

The kinetics of the process will be discussed in order to reduce the operational times for each of the involved stages, in order to increase its effectiveness. For this purpose, the duration of each stages of the process has been studied separately in order to obtain the influence of time in each mechanism. The results are shown in Table 3.

Dissolution of cobaltocene in $scCO_2$ and adsorption onto the MCM41 was performed at 70 °C and 11.0 MPa for 1, 2 and 3 h. After that, the system was slowly decompressed in order to evaluate the Co retained by the support. The amount of Co in the support after 1, 2 or 3 h of dissolution and adsorption was negligible (<0.08 wt.%). These results show that the affinity of the MCM41 by the cobaltocene is not very high, that under these conditions there is not chemisorption of the $CoCp_2$ on the MCM41, and the dissolution–adsorption rate is very slow, as it was observed in the adsorption isotherm (see Section 3.1). The interaction $CoCp_2$-$scCO_2$-MCM41 system under impregnation conditions will depend on the operational temperature and pressure, but in this work, these two factors were fixed at 70 °C and 11.0 MPa.

The effect of time in the decomposition step (stage 2) was studied at 200 °C and 14.0 MPa for 1, 2 and 3 h. The content of Co in the prepared materials was close to 3.1 wt.%, and there were not significant differences on the Co loading with time. Fig. 6 shows the progression of the metal loading versus time of the second stage for shorter and longer times. The metal loading increases with the time of the thermal degradation of the precursor reaching a maximum value of 3.4 wt.% Co at 120 min. At longer times, the cobalt content remains practically constant. This means that during approximately the first hour, the coating of the support takes place through the channels and refilling the pores of the matrix in order to form a monolayer of cobalt over the support surface. Beyond this, the kinetics is limited by another factor. Therefore in terms of Co loading, the duration of the decomposition step could be no longer than 1 h.

Finally, the complete SCFRD process was performed with the two stages in a total time of 4 h (3 h + 1 h), and a cobalt loading of 4.3 wt.% was obtained (Table 3), showing that the use of the two consecutive stages has result in a high content of cobalt in the final material.

3.3.4. Kinetics model

For a deeper understanding of what actually happens, a model that explains the physics of the process is proposed. This process has been explained as serial reaction kinetics, based on the two sequential steps of the SCFRD method:

$$A \overset{scCO_2}{\longleftarrow} B \quad \text{(RQ.1)}$$

$$B \overset{\Delta T}{\longleftarrow} D \quad \text{(RQ.2)}$$

where A is the organometallic precursor in solid state, B is the precursor dissolved into $scCO_2$ and D represents the nanoparticles adsorbed over the support.

All kinetics are considered of the first order. If the process takes place in a well-mixed batch reactor without variation in volume, the following balances can be considered:

$$\frac{dC_A}{dt} = r_2 - r_1 \approx -k_1 \cdot C_A \quad (5)$$

$$\frac{dC_B}{dt} = r_1 - r_2 - r_3 \approx k_1 \cdot C_A - k_3 \cdot C_B \quad (6)$$

$$\frac{dC_D}{dt} = r_3 \approx k_3 \cdot C_B \quad (7)$$

Talking into account that the equilibrium is displaced to the species B in the first reaction due to the solubility of the precursor in $scCO_2$ and considering the initial concentration of A is C_{A0}, the integration of (Eq. (5)) is as follows:

$$\int_{C_{A0}}^{C_A} \frac{dC_A}{C_A} = -k_1 \int_0^t dt \quad (8)$$

$$C_A = C_{A0} \cdot \exp(-k_1 \cdot t) \quad (9)$$

On the other hand, the dependence of the concentration C_B with time can be determined by combining the mass balance (Eq. (6)) and the above equation which indicates the change in C_A with time (Eq. (9)):

$$\frac{dC_B}{dt} + k_3 \cdot C_B = k_1 \cdot C_{A0} \cdot \exp(-k_1 \cdot t) \quad (10)$$

$$C_B = \frac{k_1 \cdot C_{A0}}{(k_3 - k_1)}[\exp(-k_1 \cdot t) - \exp(-k_3 \cdot t)] + C_{B0} \cdot \exp(-k_3 \cdot t) \quad (11)$$

Finally, the concentration Cd can be obtained by means of the global balance:

$$C_{A0} + C_{B0} + C_{D0} = C_A + C_B + C_D \quad (12)$$

$$C_D = C_{A0} + C_{B0} + C_{D0} \cdot \left[1 - \frac{k_3}{(k_3 - k_1)} \cdot \exp(-k_1 \cdot t)\right] + \left[\frac{k_1 \cdot C_{A0}}{(k_3 - k_1)} - C_{Bo}\right] \cdot \exp(-k_3 \cdot t) \quad (13)$$

According to this model, being $C_{B0} = C_{D0} = 0$, the concentration of the precursor in solid state (specie A), decrease exponentially;

Table 4
Cobalt loading (wt.% Co) after successive batches.

Batch number	wt.% Co
1	3.24
2	4.40
3	6.00

while the specie B has a maximum because of, on one hand it is created by dissolving the precursor in $scCO_2$, and at the same time, it disappears by effect of the temperature, precipitating the metal particles on the substrate and forming the specie D. Fig. 6 shows also the suggested model of the two serial reactions adjusted to experimental data.

As it can be seen from the values of the kinetics constants (k), it can be drawn again that the first step of dissolution is very fast compared to the adsorption stage and not limiting for the process. Thereupon, basing on the results obtained in this section, it is established an optimal operational time of 1 h.

Summarizing, the optimal conditions for the incorporation of cobalt on the MCM41 substrate in this batch configuration, takes place in unique stage at 200 °C, 14 MPa during 1 h. Dissolution takes place during the heating up period of the batch, and a previous stage of adsorption is not indicated since the adsorption in this system is not favourable. It is noteworthy that these working conditions of temperature and pressure are quite softer than these recommended by Hunde and Watkins [37] for film formation from $CoCp_2$ onto native oxide of silica wafer, which operated with temperatures above 285 °C and pressures up to 26 MPa.

3.3.5. Sequential loadings

Up to now, the cobalt loading reached was close to 3 wt.%. But it would be interesting to have higher Co content for catalytic applications where the increase of the cobalt content improves the activity. For this reason, consecutive sequential loadings have been carried out in order to obtain a powder with higher amount of cobalt. Table 4 shows the amount of cobalt achieved after each batch during 1 h per batch.

The results indicate that each batch produces 26% of gain in the cobalt load. In this way, it is possible to get a material Co/MCM41 with 6 wt.% of cobalt after three batches.

3.4. Characterization of the Co/MCM41 material

In order to identify the cobalt species that was incorporated into the support, a physicochemical characterization has been performed for the material obtained in a 4 h process: 3 h of dissolution and impregnation at 70 °C and 11.0 MPa followed by 1 h of decomposition at 200 °C and 14.0 MPa. This material has a content of cobalt of 4.3 wt.% and its characterization in summarized in the present section.

N_2 adsorption–desorption isotherms of the support and Co/MCM41 sample are shown in Fig. 7. Both solids showed type IV adsorption isotherms, which is typical of mesoporous materials, with a sharp inflection at relative pressures $P/P^{\circ} > 0.3$ which indicates the uniformity of size distribution of mesopores. BET surface of the MCM41 material is 1295 $m^2\,g^{-1}$. The pore size distributions were studied using de BJH method. Analysis of the adsorption branch gave a narrow pore size distribution with a maximum at 4.6 nm. With the incorporation of 4.3 wt.% Co, the BET surface and pore size slightly decrease to 1034 $m^2\,g^{-1}$ and 3.9 nm, respectively. Estimated pore volume of the MCM41 support is 0.196 $cm^3\,g^{-1}$ whereas for the Co/MCM41 composite material this volume decreases up to 0.156 $cm^3\,g^{-1}$ due to the presence of cobalt particles within the pores.

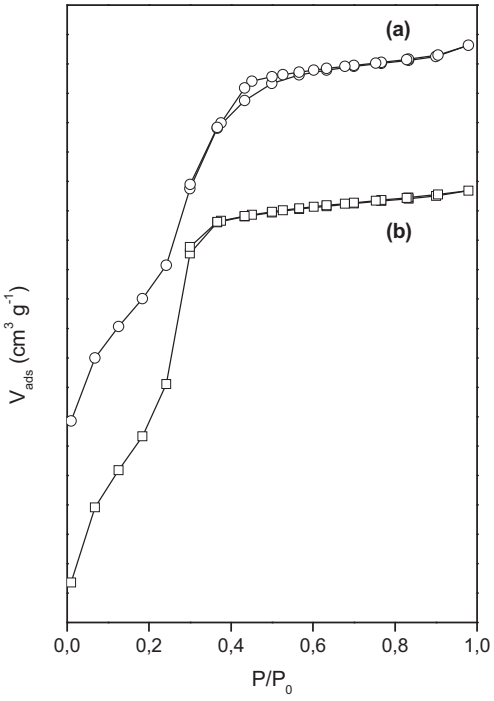

Fig. 7. N_2 adsorption–desorption isotherms obtained for (a) MCM41 and (b) Co(4.3)/MCM41.

Fig. 8 shows the XRD data of the pure $CoCp_2$ (Fig. 8a), MCM41 support (Fig. 8b) and the composite material Co(4.3)MCM41 (Fig. 8c). The diffractogram obtained for the pure precursor indicates that the cobaltocene is a highly crystalline compound with their main peaks of diffraction at 15°, 17.5°, 19.3°, 22.7°, 25°, 51.4° and 61.3°. The mesoporous MCM41 support, shows only the corresponding halo to the amorphous SiO_2 (Fig. 8b). However, the diffraction peaks corresponding to Co_3O_4 species are evident for Co/MCM41 at values of 2θ of 31.5° and 38° (Fig. 8c). There are no reflections indicating the presence of metallic cobalt particles. In Fig. 9 the FTIR spectra of the MCM41 (Fig. 9a) and Co/MCM41 (Fig. 9b) diluted in KBr are depicted. The signal at 971 cm^{-1} is due to the asymmetric stretching vibration of terminal or surface Si—O groups. Several authors reported a shift in the absorption

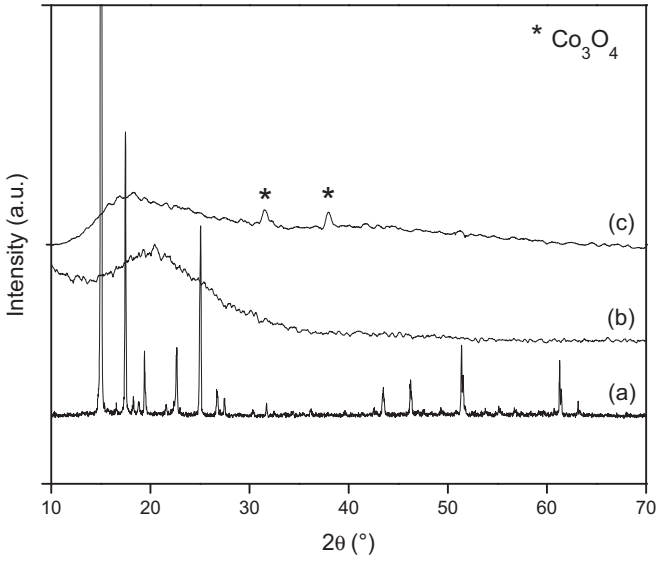

Fig. 8. XRD results of (a) pure $CoCp_2$, (b) MCM41 support and (d) Co (4.3)/MCM41.

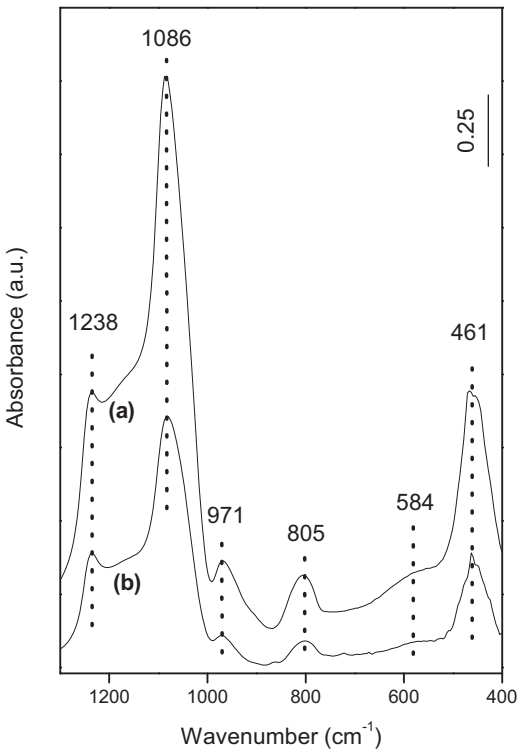

Fig. 9. FTIR spectra of the samples: (a) MCM41 and (b) Co(4.3)MCM41 diluted in KBr.

band at 971 cm^{-1} due to the substitution of silicon by ions of different metals [56]. In this regard, Hiu and Chao [57] observed a shift towards lower wavenumbers of the band corresponding to the asymmetric stretching vibration of Si—O—M, where M represents a metal ion. The shift was attributed to increased mean distance from the Si—O bond in the walls caused by the substitution of silicon by metal ions, such as Al, Na, Ti or Fe [58,59]. FTIR spectra of the Co/MCM41 (Fig. 9), exhibited no difference in the band at 971 cm^{-1}, as a consequence of the incorporation of cobalt to mesoporous support by SCFRD process. This indicates that the cobalt is not part of the MCM41 structure, however is supported on the mesoporous structure.

3.5. Residual deposits

One of the important advantages of the SCFRD process is that it does not leave any residue on the support, by the simple removal of the solvent from the substrate by controlled decompression. Therefore, after every experiment, decomposition and deposition stage, the reactor was depressurized through a needle valve for 30 min.

The presence or absence of residual deposits inside the mesoporous support after the SCFRD process, was determined through TGA analysis in air flow. The TGA results of pure $CoCp_2$ and Co(4.3)MCM41 are shown in Fig. 10.

TGA of pure precursor showed that $CoCp_2$ decomposition completely at 192 °C at atmospheric pressure. In the case of the sample impregnated with $CoCp_2$, weight losses at temperatures lower 100 °C are due to adsorbed water and represent a percentage below 5% of mass. However, an additional peak at 370 °C is observed, which is corresponding to a mass loss 33.4%.

This peak at higher temperature in comparison with the pure $CoCp_2$, reflects the presence of a different compound in the composite material and could indicate the partial decomposition of $CoCp_2$ on the MCM41 support, in concordance with the results obtained by FTIR. Weight loss in the Co/MCM41 sample is not well defined as in pure precursor, indicating desorption of the intermediate compounds of the precursor decomposition from the MCM41 channels. Also, the Co/MCM41 sample has no mass loss due to the decomposition of the precursor, which is indicative that the residual precursor is completely eliminated from the final material.

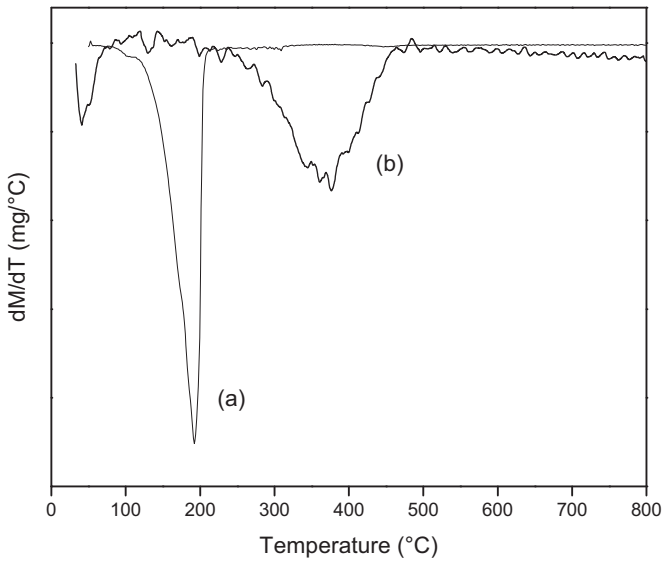

Fig. 10. TGA of (a) pure $CoCp_2$ and (b) Co(4.3)/MCM41.

4. Conclusions

Cobalt oxide nanoparticles have been deposited successfully on a MCM41 support by the SCFRD process using cobaltocene as metallic precursor. It has been determined that the adsorption isotherm of $CoCp_2$ on MCM41 is concave upward (type III), characteristic of low adsorbate–adsorbent interactions. $CoCp_2$ dissolution and adsorption at 70 °C and 11.0 MPa have shown the low affinity of this precursor by the support, obtaining cobalt loadings below 1 wt.% after 3 h. A thermal decomposition of cobaltocene in a second stage is necessary to reach higher loadings. In this step, a temperature of 200 °C is enough for the precursor decomposition and the amount of deposited Co does not depend on time in the range 1–3 h. The modelling of the SCFRD process reveals that dissolution is very fast compared to the adsorption of cobaltocene on MCM41, and that Co content is maximum after 1 h of decomposition at 200 °C and 14 MPa.

Acknowledgements

Authors gratefully acknowledge the financial support of MINECO (Spain) through the Research Project CTQ2011-27347. A. Sastre thanks Junta Castilla y León and UVa for financial support through a PIRTU contract.

References

[1] S.M. Morris, P.F. Fulvio, M. Jaroniec, Ordered mesoporous alumina-supported metal oxides, J. Am. Chem. Soc. 130 (2008) 15210–15216.
[2] N. Kumar, E. Leino, P. Mäki-Arvela, A. Aho, M. Käldström, M. Tuominen, P. Laukkanen, K. Eränen, J.-P. Mikkola, T. Salmi, D.Y. Murzin, Synthesis and characterization of solid base mesoporous and microporous catalysts: influence of the support, structure and type of base metal, Microporous Mesoporous Mater. 152 (2012) 71–77.
[3] X. Huang, W. Dong, G. Wang, M. Yang, L. Tan, Y. Feng, X. Zhang, Synthesis of confined Ag nanowires within mesoporous silica via double solvent technique and their catalytic properties, J. Colloid Interface Sci. 359 (2011) 40–46.
[4] C.T. Kresge, M.E. Leonowicz, W.J. Roth, J.C. Vartuli, J.S. Beck, Ordered mesoporous molecular sieves synthesized by a liquid-crystal template mechanism, Nature 359 (1992) 710–712.

[5] A.M.B. Furtado, Y. Wang, T. Grant Glover, M. Douglas LeVan, MCM-41 impregnated with active metal sites: synthesis, characterization, and ammonia adsorption, Microporous Mesoporous Mater. 142 (2011) 730–739.
[6] M. Li, K.N. Hui, K.S. Hui, S.K. Lee, Y.R. Cho, H. Lee, W. Zhou, S. Cho, C.Y.H. Chao, Y. Li, Influence of modification method and transition metal type on the physicochemical properties of MCM-41 catalysts and their performances in the catalytic ozonation of toluene, Appl. Catal. B: Environ. 107 (2011) 245–252.
[7] P. Stathi, K. Dimos, M.A. Karakassides, Y. Deligiannakis, Mechanism of heavy metal uptake by a hybrid MCM-41 material: surface complexation and EPR spectroscopic study, J. Colloid Interface Sci. 343 (2010) 374–380.
[8] S. Vichaphund, D. Aht-ong, V. Sricharoenchaikul, D. Atong, Production of aromatic compounds from catalytic fast pyrolysis of Jatropha residues using metal/HZSM-5 prepared by ion exchange and impregnation methods, Renew. Energy 79 (2015) 28–37.
[9] R.A. Feldman, J.M. Fraile, The influence of alumina phases on the performance of the Pd–Ag/Al_2O_3 catalyst in tail-end selective hydrogenation of acetylene, Appl. Catal. A: Gen. 502 (2015) 166–173.
[10] E. Dündar-Tekkaya, M. Türk, Effect of loading bimetallic mixture of Ni and Pd on hydrogen storage capacity of MCM-41, Int. J. Hydrogen Energy 40 (2015) 7636–7643.
[11] C. Erkey, Preparation of metallic supported nanoparticles and films using supercritical fluid deposition, J. Supercrit. Fluids 47 (2009) 517–522.
[12] S. Müller, M. Türk, Production of support gold and gold-silver nanoparticles by supercritical fluid reactive deposition: effect of substrate properties, J. Supercrit. Fluids 96 (2015) 287–297.
[13] S.E. Bozbag, L.C. Zhang, M. Aindow, C. Erkey, Adsorption of Pt(cod)me_2 onto organic aerogels from supercritical solutions for the synthesis of supported platinum nanoparticles, J. Supercrit. Fluids 66 (2012) 265–273.
[14] Q.-Q. Xu, C.-J. Zhang, X.-Z. Zhang, J.-Z. Yin, Y. Liu, Controlled synthesis of Ag nanowires and nanoparticles in mesoporous silica using supercritical carbon dioxide and co-solvent, J. Supercrit. Fluids 62 (2012) 184–189.
[15] J. Morère, M.J. Tenorio, M.J. Torralvo, C. Pando, J.A.R. Renuncio, A. Cabañas, Deposition of Pd into mesoporous silica SBA-15 using supercritical carbon dioxide, J. Supercrit. Fluids 56 (2011) 213–222.
[16] J.J. Watkins, T.J. McCarthy, Polymer/metal nanocomposite synthesis in supercritical CO_2, Chem. Mater. 7 (1995) 1991–1994.
[17] J.M. Blackburn, D.P. Long, A. Cabañas, J.J. Watkins, Deposition of conformal copper and nickel films from supercritical carbon dioxide, Science 294 (2001) 141–145.
[18] S. Wolff, M. Crone, T. Muller, M. Enders, S. Bräse, M. Türk, Preparation of Pt nanoparticles by supercritical fluids reactive deposition: influence of precursor, substrate and pressure on product properties, J. Supercrit. Fluids 95 (2014) 588–596.
[19] K. Goren, O.B. Okan, L. Chen, L.S. Schadler, R. Ozisik, Supercritical carbon dioxide assisted dispersion and distribution of silica nanoparticles in polymers, J. Supercrit. Fluids 67 (2012) 108–113.
[20] B. Wong, S. Yoda, S.M. Howdle, The preparation of gold nanoparticles composites using supercritical carbon dioxide, J. Supercrit. Fluids 42 (2007) 282–287.
[21] Q. Wang, D.F. Shantz, Ordered mesoporous silica-based inorganic nanocomposites, J. Solid State Chem. 181 (2008) 1659–1669.
[22] V.G. Milt, M.A. Ulla, E.A. Lombardo, Zirconia-supported cobalt as a catalyst for methane combustion, J. Catal. 200 (2001) 241–249.
[23] L.F. Liotta, G. Di Carlo, G. Pantaleo, G. Deganello, Catalytic performance of Co_3O_4/CeO_2 and Co_3O_4/CeO_2–ZrO_2 composite oxides for methane combustion: influence of catalyst pretreatment temperature and oxygen concentration in the reaction mixture, Appl. Catal. B: Environ. 70 (2007) 314–322.
[24] J. Llorca, N. Homs, J. Sales, P.R. de la Piscina, Efficient production of hydrogen over supported cobalt catalysts from ethanol steam reforming, J. Catal. 209 (2002) 306–317.
[25] J. Llorca, N. Homs, J. Sales, J.-L.G. Fierro, P.R. de la Piscina, Effect of sodium addition on the performance of Co-ZnO-bases catalysts for hydrogen production from bioethanol, J. Catal. 222 (2004) 470–480.
[26] W. Raróg-Pilecka, E. Miskiewiscz, M. Matyszek, Z. Kaszkur, L. Kepinski, Z. Kowalczky, Carbon-supported cobalt catalyst for ammonia synthesis: effect of preparation procedure, J. Catal. 237 (2006) 207–210.
[27] J.M. Fox III, The different catalytic routes for methane valorization: an assessment of processes for liquid fuels, Catal. Rev.: Sci. Eng. 35 (1993) 169–212.
[28] H. Schulz, Short history and present trends of Fischer–Tropsch synthesis, Appl. Catal. A: Gen. 186 (1999) 3–12.
[29] G.P. Van der Laan, A.A.C.M. Beenackers, Kinetics and selectivity of the Fischer–Tropsch synthesis: a literature review, Catal. Rev.: Sci. Eng. 41 (1999) 255–318.
[30] A.Y. Khodakov, S. Chu, P. Fongarland, Advances in the development of novel cobalt Fischer–Tropsch catalysts for synthesis of long-chain hydrocarbons and clean fuels, Chem. Rev. 107 (2007) 1692–1744.
[31] K. Hadjiivanov, V. Avreyska, G. Tzvetkov, P. Stefanov, C. Chupin, C. Mirodatos, T. Marinova, Selective catalytic reduction of NOx by methane over So/ZrO_2 catalysts, Surf. Interface Anal. 32 (2001) 175–178.
[32] M.M. Yung, E.M. Holmgreen, U.S. Ozkan, Cobalt-based catalysts supported on titania and zirconia for the oxidation of nitric oxide to nitrogen dioxide, J. Catal. 247 (2007) 356–367.
[33] I.D. Lick, A. Carrascull, M. Ponzi, E.N. Ponzi, I.L. Botto, Structural aspects of the Co/ZrO_2 catalytic system: effect of the chemical synthesis, Mater. Chem. Phys. 92 (2005) 327–332.
[34] J. Jansson, A.E.C. Palmqvist, E. Fridell, M. Skoglundh, L. Österlund, P. Thormählen, V. Langer, On the catalytic activity of Co_3O_4 in low-temperature CO oxidation, J. Catal. 211 (2002) 387–397.
[35] Y. Chen, D. Ciuparu, S. Lim, Y. Yang, G.L. Haller, L. Pfefferle, Synthesis of uniform diameter single-wall carbon nanotubes in Co-MCM-41: effects of the catalyst prereduction and nanotube growth temperatures, J. Catal. 225 (2004) 453–465.
[36] Y. Chen, D. Ciuparu, S. Lim, Y. Yang, G.L. Haller, L. Pfefferle, Synthesis of uniform diameter single wall carbon nanotubes in Co-MCM-41: effects of CO pressure and reaction time, J. Catal. 226 (2004) 351–362.
[37] E.T. Hunde, J.J. Watkins, Reactive deposition of cobalt and nickel films from their metallocenes in supercritical carbon dioxide solution, Chem. Mater. 16 (2004) 498–503.
[38] M.J. Tenorio, C. Pando, J.A.R. Renuncio, J.G. Stevens, R.A. Bourne, M. Poliakoff, A. Cabañas, Adsorption of Pd(hfac)$_2$ on mesoporous silica SBA-15 using supercritical CO_2 in its role in the performance of Pd-SiO_2 catalyst, J. Supercrit. Fluids 69 (2012) 21–28.
[39] S.E. Bozbag, N.S. Yasar, L.C. Zhang, M. Aindow, C. Erkey, Adsorption of Pt(cod)me_2 onto organic aerogels from supercritical solutions for the synthesis of supported platinum nanoparticles, J. Supercrit. Fluids 56 (2011) 105–113.
[40] O. Aschenbrenner, N. Dahmen, K. Schaber, E. Dinjus, Adsorption of dimethyl(1,5-cyclooctadiene) platinum on porous support in supercritical carbon dioxide, Ind. Eng. Chem. Res. 47 (2008) 3150–3155.
[41] S.G. Aspromonte, A. Sastre, A.V. Boix, M.J. Cocero, E. Alonso, Cobalt oxide nanoparticles on mesoporous MCM-41 and Al-MCM-41 by supercritical CO_2 deposition, Microporous Mesoporous Mater. 148 (2012) 53–61.
[42] À. Szegedi, Z. Kónya, D. Méhn, E. Solymár, G. Pál-Borbély, Z.E. Horváth, L.P. Biró, I. Kiricsi, Spherical mesoporous MCM-41 materials containing transition metals: synthesis and characterization, Appl. Catal. A: Gen. 272 (2004) 257–266.
[43] O. Aschenbrenner, S. Kemper, N. Dahmen, K. Schaber, E. Dinjus, Solubility of β-diketonates, cyclopentadienyls and cyclooctadiene complexes with various metals in supercritical carbon dioxide, J. Supercrit. Fluids 41 (2007) 179–186.
[44] W. Kast, Physical adsorption on heterogeneous solids, Chem. Ing. Tech. 61 (1989) 766.
[45] A. Cavazzini, G. Bardin, K. Kaczmarski, P. Szabelski, M. Al-Bokari, G. Guiochon, Adsorption equilibra of butyl- and amylbenzene on monolithic silica-based columns, J. Chromatogr. A 957 (2002) 111–126.
[46] B. Kayranli, Adsorption of textile dyes onto iron based water works sludge from aqueous solution: isotherm, kinetics and thermodynamics study, Chem. Eng. J. 173 (2011) 782–791.
[47] I. Kikic, P. Alessi, A. Cortesi, S.J. Macnaughton, N.R. Foster, B. Spicka, An experimental study of supercritical adsorption equilibra of salicylic acid on activated carbon, Fluid Phase Equilib. 117 (1996) 304–311.
[48] P. Subra, A. Vega-Bancel, E. Reverchon, Breakthrough curves and adsorption isotherms of terpene mixtures in supercritical carbon dioxide, J. Supercrit. Fluids 12 (1998) 43–57.
[49] P. López-Aranguren, J. Fraile, L.F. Vega, C. Domingo, Regenerable solid CO_2 sorbents prepared by supercritical grafting of aminoalkoxysilane into low-cost mesoporous silica, J. Supercrit. Fluids 85 (2014) 68–80.
[50] C. domingo, J. García Carmona, M.A. Fanovich, J. Llibre, R. Rodriguez Clemente, Single or two-solute adsorption process at supercritical conditions: an experimental study, J. Supercrit. Fluids 21 (2001) 147–157.
[51] J. Samuelson, T. Undin, T. Fornstedt, Expanding the elution by characteristic point method for determination of various types of adsorption isotherm, J. Chromatogr. A 1218 (2011) 3737–3742.
[52] S. Brunauer, P.H. Emmet, E. Teller, Adsorption of gases in multimolecular layers, J. Am. Chem. Soc. 60 (1938) 309–319.
[53] E. Maslowsky Jr., Vibrational Spectra of Organometallic Compounds, Wiley, New York, 1977 (Chapter 3).
[54] D.G. Clerc, D.A. Cleary, Fourier transform infrared spectroscopic studies of charge-transfer intercalation, Chem. Mater. 4 (1992) 1344–1348.
[55] O.G. Garkusha, B.V. Lokshin, G.K. Borisov, Vibrational spectra and structure of dicyclopentadienylzinc, J. Organomet. Chem. 553 (1998) 59–65.
[56] W. Gac, A. Derylo-Marczewskab, S. Pasieczna-Patkowska, N. Popivnyak, G. Zukocinski, The influence of the preparation methods and pretreatment conditions on the properties of Ag-MCM-41 catalysts, J. Mol. Catal. A: Chem. 268 (2007) 15–23.
[57] K.S. Hui, C.Y.H. Chao, Synthesis of MCM-41 from coal fly ash by a green approach: influence of synthesis pH, J. Hazard. Mater. 137 (2006) 1135–1148.
[58] L.Z. Wang, J.L. Shi, J. Yu, D.S. Yan, Synthesis of nanostructured mesoporous silica materials containing manganese, Nanostruct. Mater. 10 (1998) 1289–1299.
[59] S. Vetrivel, A. Pandurangan, Side-chain oxidation of ethylbenzene with tert-butylhydroperoxide over mesoporous Mn-MCM41 molecular sieves, J. Mol. Catal. A: Chem. 217 (2004) 165–174.